Bimetallic Ruthenium Nitrosyl Complexes with Enhanced Two-Photon Absorption Properties for Nitric Oxide Delivery

Yael Juarez-Martinez, Pablo Labra-Vázquez, Alejandro Enríquez-Cabrera, Andrés Leon-Rojas, Diego Martínez-Bourget, Pascal Lacroix, Marine Tassé, Sonia Mallet-Ladeira, Norberto Farfán, Rosa Santillan, et al.

Bimetallic Ruthenium Nitrosyl Complexes with Enhanced Two-Photon Absorption Properties for Nitric Oxide Delivery

Yael Juarez-Martinez[a], Pablo Labra-Vázquez[a,b], Alejandro Enríquez-Cabrera[a,b], Andrés F. Leon-Rojas[a] , Diego Martínez-Bourget[a], Pascal G. Lacroix[a]*, Marine Tassé[a], Sonia Mallet-Ladeira[a], Norberto Farfán[b], Rosa Santillan[c], Gabriel Ramos-Ortiz[d]*, Jean-Pierre Malval[e], Isabelle Malfant[a]*

Abstract: One monometallic and three bimetallic ruthenium nitrosyl (RuNO) complexes are presented and fully characterized in reference to a parent monometallic complex of formula $[FTRu(bpy)(NO)]^{3+}$, where FT is a fluorenyl-substituted terpyridine ligand, and bpy the 2,2'-bipyridine. These new complexes are built with the new ligands FFT, TFT, TFFT, and TF-CC-TF (where an alkyne C≡C group is inserted between two fluorenes). The crystal structures of the bis-$RuNO_2$ and bis-RuNO complexes built from the TFT ligand are presented. The evolution of the spectroscopic features (intensities and energies) along the series, at one-photon absorption (OPA) correlates well with the TD-DFT computations. A spectacular effect is observed at two-photon absorption (TPA) with a large enhancement of the molecular cross-section (σ_{TPA}), in the bimetallic species. In the best case, σ_{TPA} is equal to 1523 ± 98 GM at 700 nm, in the therapeutic window of transparency of biological tissues. All compounds are capable of releasing $NO^{\bullet}$ under irradiation, which leads to promising applications in TPA-based drug delivery.

Keyword: density functional calculations, ligand design, photochemistry, ruthenium nitrosyl, two-photon absorption.

[a] *Y. Juarez-Martinez, Dr. Labra-Vázquez, Dr. A. Enríquez-Cabrera, A. F. Leon-Rojas, D. Martínez-Bourget, Dr. P. G. Lacroix, M. Tassé, S. Mallet-Ladeira, Prof. I. Malfant*
Laboratoire de Chimie de Coordination du CNRS, 205 route de Narbonne, F-31077 Toulouse, France.
E-mail : pascal.lacroix@lcc-toulouse.fr, isabelle.malfant@lcc-toulouse.fr
https://www.lcc-toulouse.fr/molecules-et-composites-pour-loptique-equipe-r-2/

[b] *Dr. Labra-Vázquez, Dr. A. Enríquez-Cabrera, Dr. N. Farfán*
Facultad de Química, Departamento de Química Orgánica, Universidad Nacional Autónoma de México, 04510 México D.F., México.

[c] *Dr. R. Santillan*
Departamento de Química, Centro de Investigación y de Estudios del IPN, CINVESTAV, Apdo., Postal 14-740, México, D.F., 07000, México.

[d] *Dr. G. Ramos-Ortiz*
Centro de Investigaciones en Óptica (CIO) A.P. 1-948, 37000 León, Gto. México.
E-mail : garamoso@cio.mx
https://www.cio.mx/investigadores/gabriel_ramos/en/

[e] *Prof. J. P. Malval*
Institut de Science des Matériaux de Mulhouse CNRS-UMR 7361, Université de Haute Alsace, 15 rue Jean Starcky, 68057, Mulhouse, France.

Introduction

An intense research activity has been devoted to nitric oxide (radical NO•), since it was identified as the endothelium-derived relaxing factor by Ignarro and Palmer, in 1987.[1,2] Furthermore, NO• has been gradually recognized for its numerous physiological roles, and potential therapeutic applications.[3-5] In this context, exogenous NO• donors have been widely investigated, but they must be able to deliver NO• locally and quantitatively to avoid undesirable effect on untargeted cells.[6]

Along this line, ruthenium nitrosyl (RuNO) complexes appear particularly promising in relation to their capability to release NO• under irradiation in the λ = 300-500 nm domain, exclusively, taking advantage of the non-invasive and highly controllable characteristics of light.[7-10] However, and to be fully applicable, the NO• release should be achieved in the λ = 600 – 1 300 nm therapeutic window of relative transparency of biological tissues.[11]

To overpass this difficulty, our group has been engaged in a research effort aimed at designing RuNO chromophores capable of releasing NO• by means of two-photon absorption (TPA). This promising technique offers various advantages: high level of spatial resolution arising from its quadratic dependence on the pulsed light intensity; possibility to replace one photon in the visible domain by two photons in the therapeutic window to gain enhanced penetration in tissues; reduced side effects due to the absence of UV radiation and to the use of ultra-short laser pulses employed in the TPA techniques.[12,13] The challenge is therefore to enhance the TPA response of the RuNO complexes by means of suitable ligand modifications.

There are basically two main families of molecular TPA materials: (*i*) the dipolar or "push-pull" chromophores in which an intense charge transfer transition arises by means of electron donor and acceptor substituents linked through a π-conjugated organic bridge and (*ii*) the multipolar (mostly centrosymmetric) chromophores of greater electronic complexity than that of the dipolar species. Our first approach was devoted to a "push-pull" RuNO complex of formula $[FTRu(bpy)(NO)]^{3+}$ (**$[RuNO\text{-}1]^{3+}$** in Scheme 1) in which FT stands for a fluorenyl-substituted terpyridine ligand, and bpy for 2,2'-bipyridine. Adding an electron-rich fluorene on the robust $[Ru(terpyridine)(bipyridine)(NO)]^{3+}$ core was motivated by the expectation of enhanced "push-pull" effect toward the strongly withdrawing nitrosyl group, and from the numerous reports of TPA properties in fluorene-based chromophores.[14] Nevertheless, our efforts to enhance the TPA capabilities of such species, by addition of alternative electron donors or insertion of CC double and triple bonds to enlarge the path of delocalization led, at best, to an increase of the cross section (σ parameter quantifying the molecular TPA response) equal to roughly 50%.[15,16] More recently, we have observed that polymetallic RuNO entities can provide a large enhancement of the TPA response, with respect to that of the parent monometallic species, which encourages the investigation of NO• donors containing more than one RuNO unit.[17]

In the present contribution, we report on an investigation of quadrupolar bimetallic RuNO species based on the **$[RuNO\text{-}1]^{3+}$** benchmark reference. The compounds under investigation are shown in Scheme 1. The manuscript is organized as follows: The synthesis, characterization and description of X-ray crystal structures available are reported first. Then, the optical properties (one-photon absorption) are presented experimentally by UV-visible spectroscopy and analyzed within the framework of the time-dependent density functional theory (TD-DFT) to clarify the origin of the transitions. In the last sections, the TPA properties of the RuNO complexes recorded by the Z-scan technique are presented with the NO release capabilities.

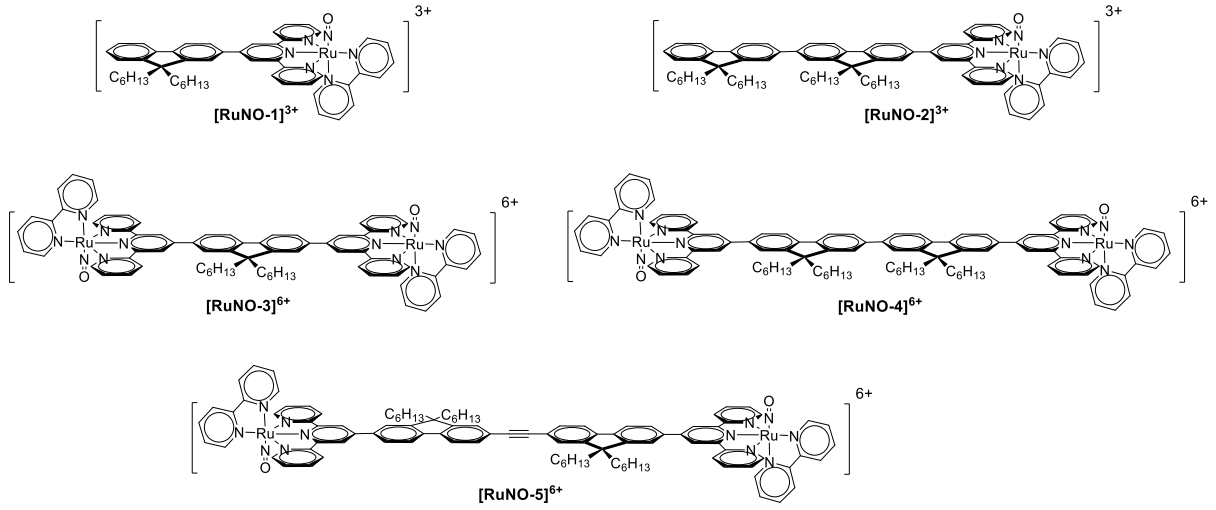

Scheme 1. Mono and di-ruthenium nitrosyl complexes under investigation.

Results and Discussion

Synthesis and characterization

Obtention of the target RuNO complexes started by the synthesis of the corresponding mono- and bis-terpyridyl ligands **L1**-**L5** which were prepared following the multi-step reaction sequences depicted in Schemes 2-3. All these ligands contain either one or two C-9 alkylated fluorenyl moieties which were chosen as the initial building blocks for the target molecules; the construction of the 2,2':6',2''-terpyridyl core was approached in every case by the Kröhnke terpyridine synthesis,[18] which is ubiquitously used for the preparation of this type of heterocycles[19] including ligand **L1**, previously investigated by our research group.[20] The synthesis starts by the aldol condensation between aldehyde **1a** and 2-acetylpyridine to give enone **2a**, which underwent the Michael addition of the enolate of pyridinium salt **3** to yield a nonisolated 1,5-dicarbonyl intermediate that cyclizes *in situ* in the presence of ammonia to give the desired terpyridyl ligand **L1**. Ligand **L2** was synthesized in a similar manner from aldehyde **1b** to give in two steps the corresponding iodinated terpyridine **4**, which was finally transformed to ligand **L2** through a Suzuki-Miyaura cross-coupling reaction with boronic acid **5**.

Bis-terpyridyl ligand **L3** has been synthesized following an alternative synthetic route to that previously described, which requires the use of 4'-bromo-2,2':6',2''-terpyridine reagents as coupling partner,[21] whose preparation suffers from tedious synthetic procedures.[22] Our approach involved the efficient formation of both terpyridine 'arms' with a 2-step Kröhnke synthesis taking place simultaneously at both sides of the fluorene backbone. Conversely, for ligands **L4**-**L5** convergent synthetic routes were envisioned as this approach is better suited for large organic molecules, frequently providing higher overall efficiencies over their divergent counterparts,[23] with related polyfluorene bis-terpyridyl ligands being indeed efficiently accessed through convergent syntheses.[24] Thus, ligands **L4** and **L5** were conveniently prepared from iodinated terpyridine **4** employing Suzuki-Miyaura and Sonogashira cross-coupling reactions, respectively, as the key final synthetic steps, with either pinacolboryl (**8**) or

acetylenic (**11**) terpyridines as coupling partners. The identity of ligands **L1-L5** and their precursors was successfully corroborated by means of $^{1}H/^{13}C$-NMR and HRMS.

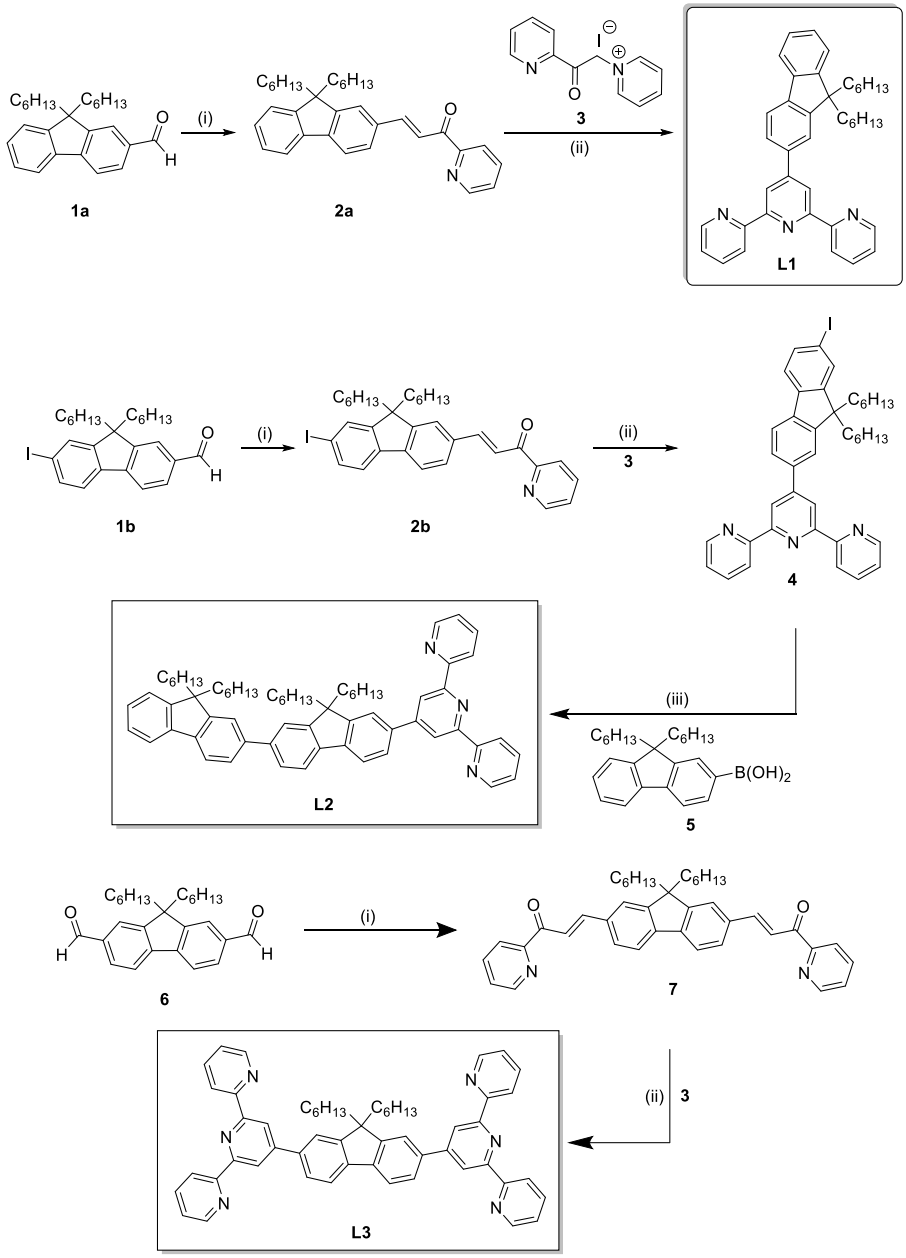

Scheme 2. Synthesis of ligands **L1-L3**. Reagents and conditions: (i) 2-acetylpyridine, NaOH, EtOH/H_2O/THF, rt (82–90 %); (ii) NH_4OAc, EtOH/THF, reflux (44–58 %); (iii) $Pd(PPh_3)_2Cl_2$, K_2CO_3, Toluene/MeOH, reflux (66 %).

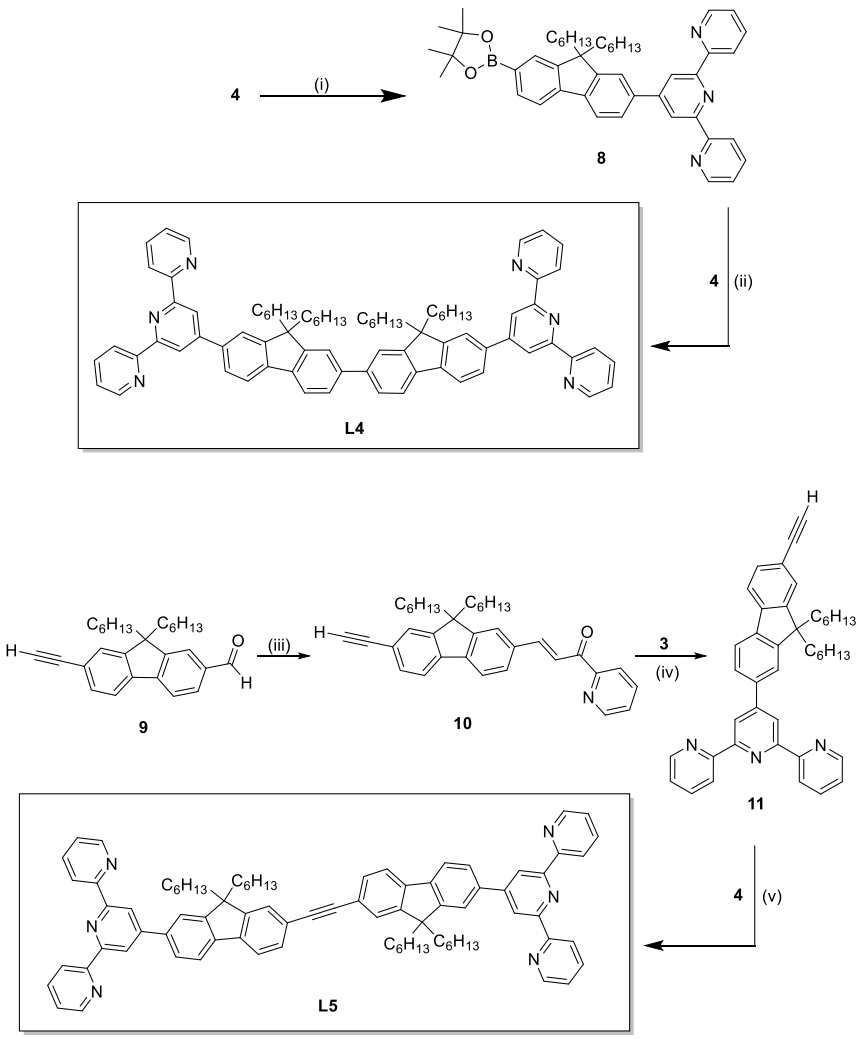

Scheme 3. Synthesis of ligands **L4-L5**. Reagents and conditions: (i) $Pd(dppf)Cl_2$·DCM, B_2pin_2, KOAc, DMSO, 110 °C (56 %); (ii) $Pd(dppf)_2Cl_2$, K_2CO_3, TBAB, Toluene/MeOH, reflux (65 %) (iii) 2-acetylpyridine, NaOH, $EtOH/H_2O/THF$, rt (93 %) (iv) NH_4OAc, EtOH/THF, reflux (68 %) (v) $Pd(PPh_3)_2Cl_2$, CuI, THF/Et_3N, reflux (72 %).

Ligands **L1-L5** were used for the preparation of the target RuNO complexes following the general 4-step synthetic route depicted in Scheme 4. The first step was the metalation with $RuCl_3$•xH_2O, which yielded neutral Ru(III) complexes **[Ru(L1-L2)Cl$_3$]** and **[Cl$_3$Ru(L3-L5)RuCl$_3$]** in high yields; the second step involved the replacement of two chlorido ligands by a 2,2'-bipyridine with the concomitant $Ru^{III} \rightarrow Ru^{II}$ reduction to yield complexes **RuCl-1** to **RuCl-5** in satisfactory yields; these key intermediates are further transformed to the final RuNO complexes by an efficient ligand exchange reaction with $NaNO_2$ to give **RuNO$_2$-1** to **RuNO$_2$-5,** which were finally treated with concentrated hydrochloric acid followed by metathesis with aqueous NH_4PF_6 to yield the target **RuNO-1** to **RuNO-5** complexes in high yields, with their FT-IR spectra showing the clear presence of ν(NO) vibrations in the ν = 1934-1940 cm^{-1} interval. In this range, the electronic configuration of Ru-NO can be considered as formally Ru^{II}-NO^+.[25]

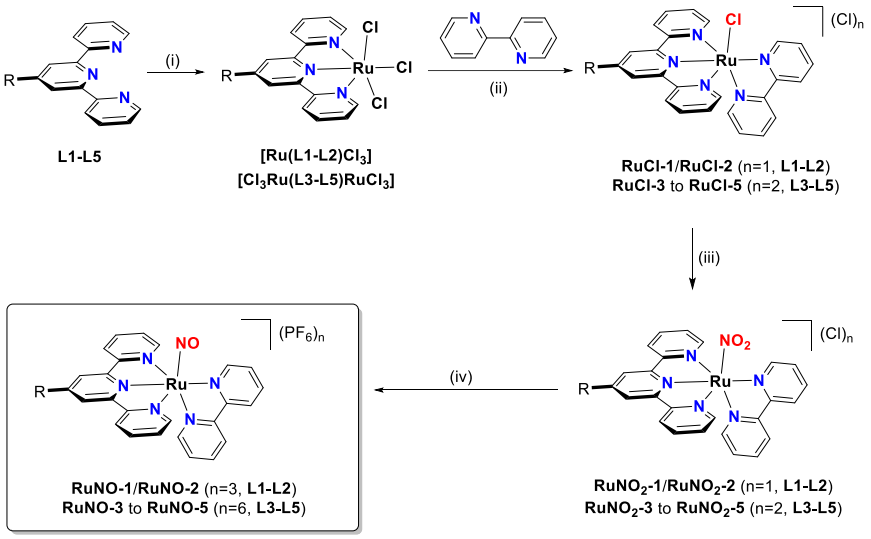

Scheme 4. Synthesis of complexes [**RuNO-1**]$^{3+}$ to [**RuNO-5**]$^{6+}$ **(**For the complete structure of ligands **L1**-**L5** see Schemes **2-3**). Reagents and conditions: (i) $RuCl_3xH_2O$, EtOH, reflux (82–96 %); (ii) LiCl, Et_3N, EtOH/H_2O, reflux (60–90 %); (iii) $NaNO_2$, EtOH/H_2O, reflux (91–99 %); (iv) HCl, EtOH, 60 °C, then $NH_4PF_{6(aq)}$ (77–91 %).

The identity of all the diamagnetic Ru^{II} complexes was corroborated by NMR and HRMS analyses, which provided a convenient way to assess the completeness of the transformations (see *Supplementary Information*).

Structures description

X-ray crystal structures were obtained for **[RuNO-3]**$(PF_6)_6$, and for **[RuNO$_2$-3]**$(PF_6)_2$, which corresponds to the last intermediate described in Scheme 4, step (iii). To the best of our knowledge, the present crystal structures are the first ones reported to date for bimetallic complexes based on the [Ru(terpy)(NO_2)] and [Ru(terpy)(NO)] cores, according to a survey in the Cambridge Crystallographic Data Centre (CCDC), showing no entries for either [Ru(terpy)(NO)] or [Ru(terpy)(NO_2)] bimetallic species.

[RuNO$_2$-3]$(PF_6)_2$ crystallizes in the $P2_1/c$ monoclinic space group. The asymmetric unit cell is built up from one bis Ru-NO_2 cationic species, two disordered PF_6^- anions, and one molecule of DMF. Therefore, the complex bears a charge 2^+, and the ruthenium atoms are assumed to be Ru^{II}. The structure of the complex is shown in Figure 1. The overall conformation of the π-conjugated subunit corresponds roughly to the C_s symmetry. More precisely, except for the disordered hexyl chains and the two anionic NO_2^- ligands, the remaining molecular structure is C_s within a tolerance of 0.9 Å, which indicates that the two coordination spheres around the ruthenium centers are roughly equivalent. The fluorene unit is planar with torsion angle between fluorene (13 heavy atoms) and terpyridine (18 heavy atoms) equal to 27.77(4)° and 32.57(4)°.

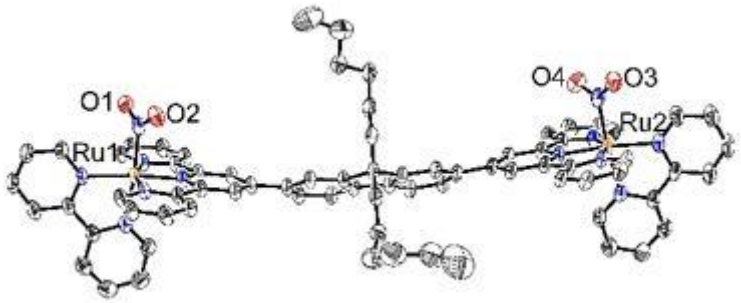

Figure 1. View of the complex **[RuNO$_2$-3]$^{2+}$**. Hydrogen atoms are omitted for clarity. Displacement ellipsoids are drawn at the 50% probability level.

[RuNO-3]$(PF_6)_6$ crystallizes in the *Pbcn* orthorhombic space group. The asymmetric unit cell is built up from one bis Ru-NO cation and six PF_6^- anions. The complex bears a charge 6+ and the RuNO fragments are linear with Ru-N-O angles equal to 176.1(5)° and 1.775(6)°. Therefore, the electronic configuration corresponds to $Ru^{II}(NO^+)$. The molecular structure of the complex is shown in Figure 2. Contrary to the **RuNO$_2$** species previously described, the present complex does not exhibit any symmetry. The fluorene appears slightly bent, with largest deviation to mean plane (13 atoms) observed at C(34) equal to 0.117 Å. In the terpyrine units the largest deviations to mean planes (18 atoms) are equal to 0.128 Å at C(7) and to 0.121 Å at C(58). Interestingly, the torsion angles between the fluorene and the two terpyridines are significantly different, with values equal to 45.21(12)° and 24.24(9)°. Details for the crystallographic data are provided as supporting information for both **[RuNO$_2$-3]**$(PF_6)_2$, and **[RuNO-3]**$(PF_6)_6$.

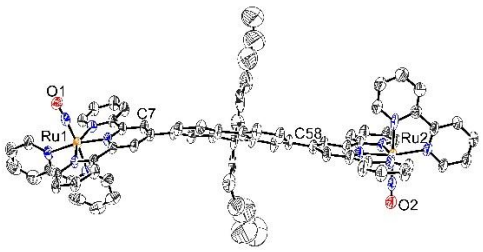

Figure 2. View of the complex **[RuNO-3]**$(PF_6)_6$, with atomic labeling scheme for the atoms of interest. Hydrogen atoms are omitted for clarity. Displacement ellipsoids are drawn at the 50% probability level.

Electronic properties

The UV-visible spectra of the five RuNO complexes recorded in MeCN are shown in Figure 3. The spectra reveal the presence of numerous transitions, which can be roughly classified in three groups as follows: a low-lying band (*A*) in a wavelength range λ = 400 – 550 nm, a multicomponent band (*B*) in the λ = 250 – 400 nm range, and a very intense band (*C*) around 200 nm. More intense bands observed at higher energy appear to be a general trend along the series. Concerning band *A*, two tendencies are clearly observed: the complexes containing two fluorenyl units (**[RuNO-2]$^{3+}$**, **[RuNO-4]$^{6+}$**, and **[RuNO-5]$^{6+}$**) are shifted to lower absorption maxima (λ_{max}) values (from 450-460 nm to 490-500 nm) and the bimetallic complexes (**[RuNO-3]$^{6+}$**, **[RuNO-4]$^{6+}$**, and **[RuNO-5)]$^{6+}$** exhibit intensities (extinction

coefficents ε) at least twice as large as those of the monometallic species (ε = 35 000 to 45 000 versus 12 000 to 17 000 M^{-1} cm^{-1}).

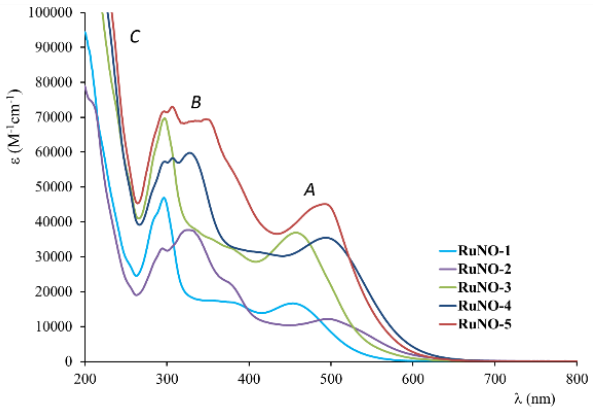

Figure 3. UV-visible absorption spectra for [**RuNO-1**]$(PF_6)_3$ – [**RuNO-5**]$(PF_6)_6$, in acetonitrile.

The optical spectra were computed by TD-DFT, to try to find a rationale for these trends. The detailed data (spectra, composition of electronic transitions) are provided in *Supporting Information*). Roughly, the five compounds exhibit a spectrum with three bands of relative intensities *A* < *B* < *C*, which substantially agrees with the experiment. In any case, the low-energy bands *A* arise from single HOMO → LUMO based transitions. Except for **[RuNO-3]$^{6+}$**, the energy shifts between computed and experimental transitions are around 1 000 cm^{-1}, which is fully satisfactory especially in the case of complexes with heavy atoms and long range charge transfers capabilities.[26] The discrepancy observed between computation and experiment in the case of **[RuNO-3]$^{6+}$** might be tentatively related to the presence of anions in strong interaction with the +6 charged complex **RuNO-3** of relatively small size in solution (UV-vis spectra). By contrast, the computations are performed on isolated cations, which necessarily introduce some difference. Interestingly, both observations (red-shift in λ_{max} for **[RuNO-2]$^{3+}$**, **[RuNO-4]$^{6+}$**, and **[RuNO-5]$^{6+}$** and increased intensities for **[RuNO-3]$^{6+}$**, **[RuNO-4]$^{6+}$**, and **[RuNO-5]$^{6+}$**) are confirmed by the computation, which allows the investigation to be conducted at the molecular level, to target the origin of the observed behaviors.

The orbitals of interest (HOMO, LUMO) are shown in Figure 4. The origin of the larger λ_{max} values observed in complexes containing two fluorene units (**[RuNO-2]$^{3+}$**, **[RuNO-4]$^{6+}$**, **[RuNO-4]$^{6+}$**) is suggested from the examination of the Figure. While the LUMO level is strictly pinned on the ruthenium nitrosyl fragment and therefore stays roughly unaffected all over the series, the HOMO level reflects the high energy of the electron-rich fluorene. Having two fluorene units in the middle of the molecules (**[RuNO-2]$^{3+}$**, **[RuNO-4]$^{6+}$**, and **[RuNO-5]$^{6+}$**) significantly enhances the donating capabilities of the ligands, which increases the energy of the HOMO level, reducing the HOMO-LUMO energy difference, and hence the energy of the transition.

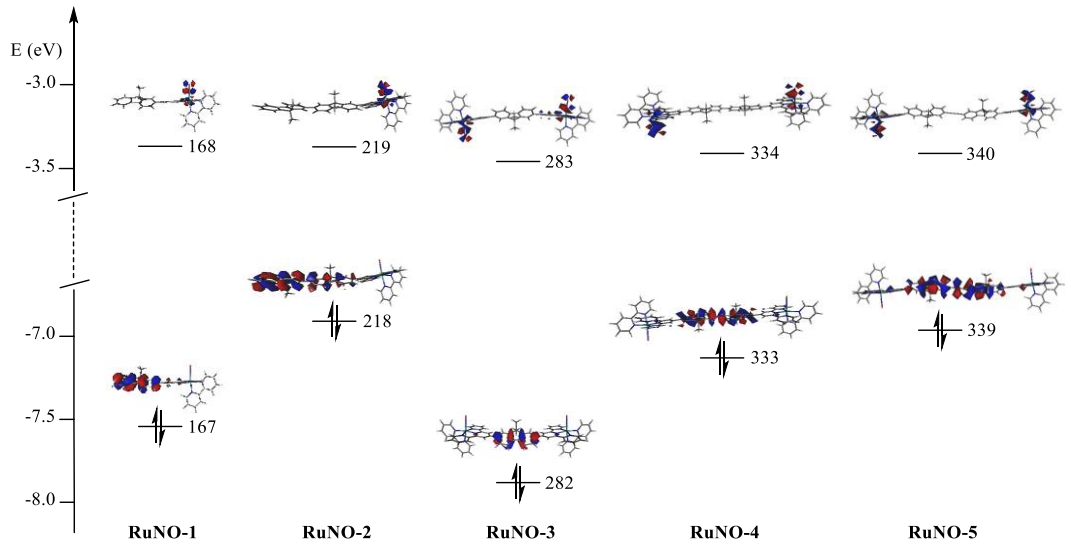

Figure 4. Frontier orbitals and relative energies computed by DFT for the five RuNO complexes.

TPA properties

The Z-scan technique was employed to quantify the TPA properties,[27] owing to the very weak photoluminescence in the infrared (*ca* 800 nm) detected in the RuNO complexes upon one-photon excitation, which precludes employing other nonlinear characterization techniques such as the two-photon excited fluorescence.[28] At the molecular level, the quantification of the TPA properties is expressed by a cross-section (σ_{TPA}), expressed in Göppert-Mayer units (1 GM = 10^{-50} cm^4 s $photons^{-1}$ $molecules^{-1}$).[12c] Z-scan experiment provides a direct access to σ_{TPA}.

The values of σ_{TPA} obtained though Z-scan experiments are gathered in Table 1. At first, the properties were measured using an incident wavelength equal to 800 nm, which is the most widely used one in biophotonics applications, due to the availability of the Ti-sapphire laser technology operating at this wavelength. Additionally, working at 800 nm allows a comparison with dipolar RuNO species previously reported,[15,16,29] in which the different attempts to enlarge the TPA response by chemical modifications lead at best to a σ_{TPA} enhancement equal to roughly 50%. In the present investigation, and by contrast to the situation encountered in dipolar complexes, the enhancement of the TPA response is more pronounced in each quadrupolar species (Table 1). In particular, σ_{TPA} reaches a value of 401 ± 40 GM at 800 nm for **[RuNO-3]$^{6+}$**.

	700 nm	800 nm	850 nm	900 nm	950 nm	1000 nm
[RuNO-1]$(PF_6)_3$	279 ± 39	115 ± 20	233 ± 50	62 ± 14	18 ± 4	34 ± 0.2
[RuNO-2] $(PF_6)_3$	662 ± 140	152 ± 13	421 ± 14	68 ± 19	34 ± 12	109 ± 18
[RuNO-3] $(PF_6)_6$	1182 ± 180	401 ± 40	452 ± 63	82 ± 24	37 ± 11	80 ± 14
[RuNO-4] $(PF_6)_6$	838 ± 250	185 ± 19	435 ± 70	87 ± 19	49 ± 18	200 ± 43
[RuNO-5] $(PF_6)_6$	1523 ± 98	309 ± 35	510 ± 63	103 ± 19	63 ± 25	229 ± 46

Table 1. TPA cross-sections (σ_{TPA} in GM)) (**[RuNO-1]**$(PF_6)_3$, **[RuNO-2]**$(PF_6)_3$, **[RuNO-3]**$(PF_6)_6$, **[RuNO-4]**$(PF_6)_6$, and **[RuNO-5]**$(PF_6)_3$) recorded at various incident wavelengths within the therapeutic window.

Two-photon electronic spectra may be significantly different than one-photon spectra, especially in the case of centrosymmetric molecules (*e.g.* **[RuNO-5]$^{6+}$**). Indeed, any forbidden transition in a one-photon absorption (OPA) process with C_i symmetry is TPA active, while any allowed OPA transition is strictly TPA silent. Although **[RuNO-4]$^{6+}$** possesses C_2 symmetry, it can be regarded as pseudo-centrosymmetric, which implies that the intense OPA transitions are allowed but necessarily weak in the TPA process. The same analysis can be transposed to **[RuNO-3]$^{6+}$**, however to a less extent, as this complex moves away from the strict centrosymmetry. Predicting the TPA spectra from the related OPA spectra is therefore impossible for the present RuNO complexes. To overpass this difficulty, different incident wavelengths were selected in the final TPA investigations from λ = 700 nm to 1000 nm to cover a large wavelength domain in the therapeutic window (Table 1). A typical trace of the normalized transmission (T(z), see experimental section) obtained by Z-scan is shown in Figure 5 (other T(z) are provided in supporting information). In all samples, the Z-scan traces exhibit good symmetry around Z = 0, and that T(z) decreases as the intensity of the pulses increases. The decrease in transmission as a function of excitation intensity shown in Figure 5 follows a monotonic linear trend, indicating that the origin of the measured nonlinearity is due to a two-photon absorption process. Further, to make sure that the Z-scan traces display only nonlinear transmission due to TPA, the samples were tested at different wavelengths under the condition where σ_{TPA} was independent of the excitation energy. The σ_{TPA} values obtained from the Z-scan traces are plotted in Figure 6.

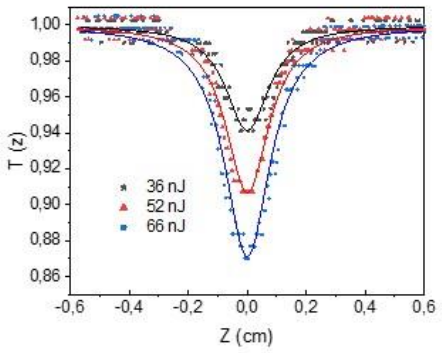

Figure 5. Normalized transmission T(Z) in Z-scan experiment at various laser pulse energies for **[RuNO-5]**$(PF_6)_6$ at λ = 800 nm. [C] = 5 10^{-3} mol L^{-1}.

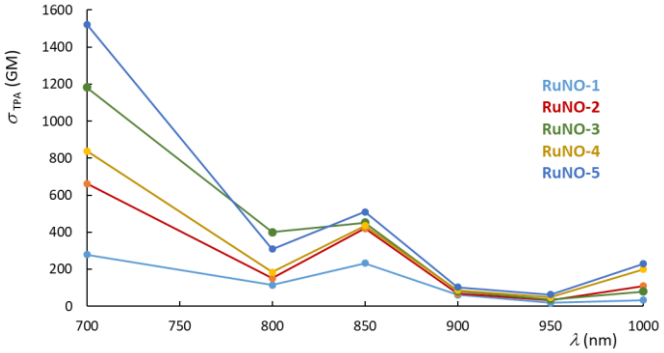

Figure 6. TPA spectra for the five RuNO complexes recorded in acetonitrile at various incident wavelengths.

The data recorded at λ = 800 nm are far from providing the largest σ_{TPA} values. For instance, the spectra present a first enhancement of TPA at λ = 850 nm and a secondary enhancement at 1000 nm. These spectra can be explained partially by the fact that in the Z-scan experiments the energy $2\hbar\omega$ of a pair of the infrared photons grossly coincides with the low-lying band *A* observed in OPA in the 400 – 550 nm wavelength range (Figure 3). At 850 nm, maximum values of σ_{TPA} in the range 435 - 510 GM were reached for the quadrupolar complexes **[RuNO-3]$^{6+}$**, **[RuNO-4]$^{6+}$, [RuNO-5]$^{6+}$**. These values practically double the value measured for the push-pull complex **[RuNO-1]$^{3+}$**. Clearly, the insertion of a second fluorenyl unit from **[RuNO-1]$^{3+}$** to **[RuNO-2]$^{3+}$** increased the nonlinearities in the push-pull complexes. Likewise, extending the π-conjugation from **[RuNO-4]$^{6+}$** to **[RuNO-5]$^{6+}$** by inserting a triple bond also increases the nonlinearities. Nevertheless, for bimetallic species the trend of increasing σ_{TPA} by inserting a second fluorenyl unit was not fully verified as it is seen by comparing **[RuNO-3]$^{6+}$** and **[RuNO-4]$^{6+}$**. Globally, the spectra of σ_{TPA} show evident trends of structure-property relationships in which the nonlinear polarizability of each of the title compounds correlates satisfactorily with their linear polarizability, *e.g.* red shifting in the OPA peak and large increments of ε upon modification to the molecular structure is also accompanied by increments in σ_{TPA}. Furthermore, the UV-vis band *B* observed in the 250 – 400 nm range seems to have its counterpart in the TPA spectra. The attempts to extend the TPA spectra to λ = 600 nm were unsuccessful because, for some of the molecules, saturation of absorption induced by OPA was detected (Figure 3). At 700 nm, a notorious enhancement in the σ_{TPA} spectra is observed. This wavelength represents the onset of linear absorption. It should be noticed that in two-photon transitions, if the energy of one photon is close to the energy of an electronic state, the nonlinearity can be enhanced notably (*vide infra* equation 2). This one-photon resonance is a well-known effect observed in organic molecules either in the degenerate case (two photons of excitation of equal energy) or nondegenerate case (two photons of different energy).[30] Such one-photon resonance enhancement can occur even without populating the intermediate level, since the excitation is resonant with such level but does not promote an electron to an excited state. In addition, we cannot discard the possibility that as the excitation is near the onset of linear absorption, the detected two-photon transitions could take place through a two-step process, where a real intermediate excited state could be involved. In Z-scan traces, the measured transmission T as a function of the sample position Z is always normalized. The normalization is performed by considering the signal measured far from the Z = 0 (for instance, at the edges of the Z-scan trace), where the nonlinearities vanish. At the edges of the Z-scan traces the nonlinear absorption does not occur and the transmission of the sample is only influenced by linear absorption effects, in case the latter are present. Normalization of data ensures that pure OPA effects are removed from Z-scan traces. Thus, the calculated values of σ_{TPA} at 700 nm are indeed due to two-photon absorption process and are free of overestimation. As some of the ruthenium complexes under study are pseudo-symmetric molecules, then the TPA process at 700 nm can potentially occur either via a virtual or real intermediate state (*vide infra* Fig. 8 for a model and the corresponding transition selection rules). Seen globally, the presented nonlinearities of the complexes are sizeable in a large wavelengths range (700 – 850 nm) and fully compatible with the therapeutic window.

At a more fundamental level, providing a rationale and full understanding of the origin of the TPA response in a molecule is a complicated task and was reported elsewhere.[12] σ_{TPA} derives from the second molecular hyperpolarizability γ,[31] which can be evaluated within the framework of the perturbation theory, and expressed by an extensive sum-over-state expression, which involves contribution of all $\langle m|\mu|n\rangle = \mu_{mn}$ transitions between states *m* and *n*, as follows:[32]

$$\gamma_{ijkl} = \frac{1}{6\hbar^3} \times P(i,j,k,l) \times \left[\sum_{m\neq 0} \sum_{n\neq 0} \sum_{p\neq 0} \frac{\langle 0|\mu_i|m\rangle \langle m|\mu_j|n\rangle \langle n|\mu_k|p\rangle \langle p|\mu_l|0\rangle}{(\omega_{m0}-\omega-i\Gamma_{m0})(\omega_{n0}-2\omega-i\Gamma_{n0})(\omega_{p0}-\omega-i\Gamma_{p0})} - \right.$$
$$\left. \sum_{m\neq 0} \sum_{n\neq 0} \frac{\langle 0|\mu_i|m\rangle \langle m|\mu_j|0\rangle \langle 0|\mu_k|n\rangle \langle n|\mu_l|0\rangle}{(\omega_{m0}-\omega-i\Gamma_{m0})(\omega_{n0}-\omega-i\Gamma_{n0})(\omega_{n0}+\omega-i\Gamma_{n0})} \right] \qquad (1)$$

In this expression, *P* is a perturbation operator, *0*, *m*, *n*, *p* are the labels of the ground and excited states, *i*, *j*, *k*, *l* are molecular axes, $\hbar\omega_{m0}$ is the energy of state *m*, and Γ_{m0} is the band width of the $0 \rightarrow m$ transition. Equation (1) encompasses the intricate contribution of millions of terms and therefore requires drastic simplifications to provide a comprehensive, however frequently oversimplified picture. In particular, the most appealing quadrupolar species (**[RuNO-3]$^{6+}$**, **[RuNO-4]$^{6+}$**, and **[RuNO-5]$^{6+}$**) may be ultimately described by a simple three states (*g*, *e*, *e'*) model, leading to the following expression:[33]

$$\sigma_{TPA} \approx \frac{4\pi^2\omega_{ge'}^2}{5\hbar^2c^2} \frac{\mu_{ge}^2\mu_{ee'}^2}{\left(\omega_{ge}-\frac{\omega_{ge'}}{2}\right)^2\Gamma'} \qquad (2)$$

in which the TPA process takes place from the ground state (*g*) to the second excited state (*e'*). The situation described in Equation (2) is depicted in Figure 8 (top). Interestingly, the presence of an intense $g \rightarrow e$ OPA transition (large transition moment μ_{ge} value) having energy $\hbar\omega_{ge}$ close to that of the incident laser beam $\frac{\hbar\omega_{ge'}}{2}$ leads to the possibility of significant cross-section enhancement due to a nearly vanishing denominator in Equation (2). For this reason, quadrupolar chromophores are usually more TPA efficient than their parent dipolar species.

This model was tentatively applied in the case of **[RuNO-5]$^{6+}$**, to account for a high σ_{TPA} value at 700 nm. Details for the discussion on the origin of the TPA response based on the present TD-DFT computations are presented in *Supporting Information*. It is finally proposed that two transitions ($1 \rightarrow 14$ and $1 \rightarrow 23$) account for the large TPA response measured for this material. Additionally, it is proposed that the most significant TPA response of **[RuNO-4]$^{6+}$** is blue shifted to wavelengths shorter than 700 nm, therefore is not present in Figure 6.

Measuring a cross-section of 1523 GM (**[RuNO-5]**$(PF_6)_6$) at 700 nm after a reference (**[RuNO-1]**$(PF_6)_3$) initially reported at 115 GM at 800 nm rises the issue of the magnitude of the highest σ_{TPA} value accessible in RuNO complexes. As is well known, any nonlinear optical phenomenon is ultimately related to intramolecular charge transfers.[34] Therefore, increasing the size of the π-delocalized skeleton becomes desirable for enhancing the molecular TPA response.[35] On the other hand, the challenge in a molecular device is not the simple optimization of the molecular property, but furthermore the possibility to introduce as many chromophores as possible in the device. In this context, the relevant factor of merit is the molecular property expressed per mass unit (σ_{TPA}/MW). As far as we know, the highest σ_{TPA}/MW value reported for ruthenium-based TPA chromophores is that of Humphrey *at al*., who observed a value of 1.46 GM mol g^{-1} for a dendrimeric structure bearing 9 bis(diphosphine)ruthenium units and a total of 25 phenyl rings.[36] In the case of the present **[RuNO-5]$^{6+}$** cation, σ_{TPA}/MW at 700 nm is equal to 0.88 GM mol g^{-1}. Furthermore, if the hexyl chains are not taken into account from the fact that they are present for the purpose of solubility only but play no direct role in the charge transfer properties, σ_{TPA}/MW reaches 1.10 GM mol g^{-1}, which corresponds roughly to 3/4 of the record value published by Humphrey.

These values lead to the conclusion that the TPA properties of the present bimetallic species are among the most efficient for ruthenium-based materials. However, designing new ruthenium-based TPA materials is not the purpose of our research program, aimed at being able to initiate the NO• release by means of two-photon processes. Along this line, the present compounds appear especially promising.

NO release

Finally, the NO• release capabilities have been tested along the RuNO series. In order to confirm the photodissociation reaction, the one photon absorption photolysis has been performed upon irradiation at 490 nm for the five RuNO complexes in acetonitrile. A representative example is provided in Figure 7 for **[RuNO-5]**$(PF_6)_6$. (see Supplementary Information for the other compounds). The band of interest is around 400-550 nm (band *A*) as it is related to the dominant contribution of the single HOMO-LUMO excitation involving fluorene - Ru(NO) charge transfer. Two opposite tendencies are clearly observed for the two complexes bearing one fluorenyl unit, namely (**[RuNO-1]**$^{3+}$, **[RuNO-3]**$^{6+}$, and the three others with two fluorenyl units (**[RuNO-2]**$^{3+}$, **[RuNO-4]**$^{6+}$, and **[RuNO-5)]**$^{6+}$). In the first case, whether mono- or bimetallic, a blue shift is observed while it is a red shift in the second case. In the five RuNO complexes the shift is around 15-25 cm^{-1} with a maximum around 475 nm. Moreover, the presence of isosbestic points indicates a clean conversion of the $Ru^{II}(NO^+)$ complexes to related photolysed species. No back-reaction is observed when the light is turned off.

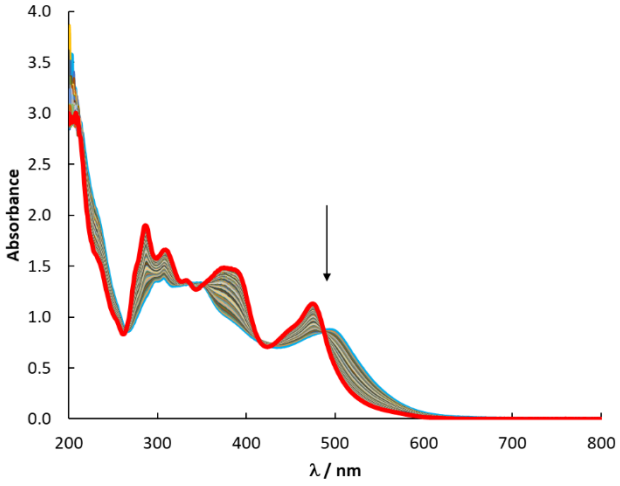

Figure 7. Evolution in the absorption spectra of [**RuNO-5**]$(PF_6)_6$ in acetonitrile under irradiation at λ=490 nm (see black arrow). Blue line: before irradiation; red line: after completeness of the photochemical process.

The ability of RuNO complexes to release nitric oxide under irradiation was mainly studied on monometallic species, according to the following equation:

$$(L)Ru^{II}\text{-}(NO^+) + \text{solvent} \xrightarrow{h\nu} (L)Ru^{III}\text{-solvent} + NO^{\cdot} \qquad (3)$$

In these cases, we have always observed the release of NO as a neutral NO·, thus leading to a subsequent $Ru^{II} \rightarrow Ru^{III}$ conversion during the release process.[15,20,29,37] In the class of complexes built up from substituted terpyridine and bipyridine ligand, we have reported on various examples of such behavior with quantum yield of photorelease (ϕ_{NO}) ranging from 0.004 to 0.03 depending on the donor substituent

and the wavelength of irradiation.[15,20,29,37] The resulting release of nitric oxide is followed by the formation of a solvent bound ruthenium(III) photoproduct, according to equation (3). This was clearly evidenced by X-ray crystallography in the case of a good stability of the Ru^{III} photo product in previous reports.[37(d),38] Nevertheless, it should be pointed out that equation (3) does not preclude any further chemical evolution of [(L)Ru^{III}(solvent)], with the outcome of a possible photoproduct different than the expected species.

In the present case of the monometallic (**RuNO-1**, **RuNO-2**) and of bimetallic (**RuNO-3** to **RuNO-5**) species, the same model was followed and successfully gave rise to the determination of ϕ_{NO}. Their values are gathered in Table 2. The model used to determine ϕ_{NO} (see Experimental Section) is based on a two-level description, which assumes that the starting complex and the final photo-product are the only absorbing species present in solution in significant concentration throughout the release process. The presence of pseudo-isosbestic points observed in the kinetics experiment (see Figure 7 and Figure 7.1.1-5 in *Supporting Information*) suggests that this assumption is acceptable. Moreover, the agreement between the experimental and theoretical points (see Figure 7.4.1-5 in *Supporting Information*), as well as the quantum yield values being within the range of values for this family of compounds strongly support this description.

Table 2. Quantum yield of photorelease (ϕ_{NO}) under irradiation at λ = 490 nm in acetonitrile for **RuNO-1-5** complexes.

	RuNO-1	**RuNO-2**	**RuNO-3**	**RuNO-4**	**RuNO-5**
ϕ_{NO}	0.0024	0.0024	0.0039	0.0030	0.0038

To confirm the formation of nitric oxide (NO•) during the photolysis, an EPR experiment was performed during this photoreaction in the presence of iron(II)-*N*-methyl-D-glucamine dithiocarbamato (Fe-MGD). This spin trap generates a Fe-MGD-NO complex with a characteristic EPR signal.[39] As shown in Figure 8, the EPR spectrum of the mixture solution of **[RuNO-5]$^{6+}$**/Fe-MGD after 10 min photolysis shows a triplet signal with a hyperfine splitting constant value of $a_N = 1.2 \times 10^{-3}$ cm^{-1} and a g-factor of g = 2.040. This EPR signal is consistent with the formation of [$(MGD)_2$-Fe^{2+}-NO] complex. If the same solution is kept initially in the dark, the presence of NO is not detected which confirms the photo-triggered character for the generation of NO. The same behavior is observed for the other Ru(NO) complexes (see figures in *Supplementary Information*).

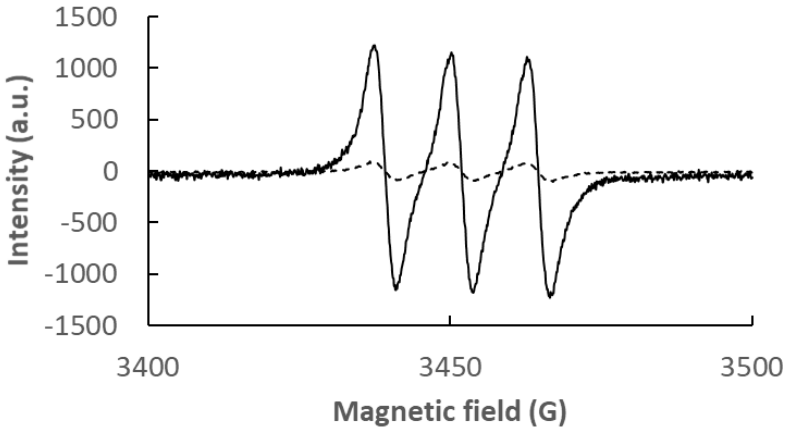

Figure 8. Triplet EPR signals from NO· trapped by [Fe(MGD)$_2$] for [**RuNO-5**](PF$_6$)$_6$ upon one photon excitation at room temperature and at λ >400 nm (Hg lamp)

To verify that the NO• release is indeed achieved under two-photon irradiation, experiments were undertaken with the Griess reagent which leads to the formation of a pink dye in the presence of NO•.[40] For this purpose an aqueous solution of **RuNO-5** (0.3 mM) in presence of Griess agent was irradiated at 980 nm through a focalized optical configuration using a *fs*-pulse laser. Note that a reference solution of **RuNO-5** without Griess agent was also irradiated in the same condition to compare the relative effects. Figure 9 shows the evolution of the absorption spectrum for each solution during the two-photon reaction. As similarly observed for the visible irradiation of **RuNO-5**, the red side of its longest wavelength absorption band progressively decreases upon the NIR excitation (see inset Figure 9A). Interestingly, in presence of Griess agent the photoreaction leads to the concomitant release of NO as clearly indicated by the significant increase of large absorption bands in the 650-750 nm range which can be ascribed to the generation of the corresponding 'azo' dye by-product.[37(d),41] We therefore demonstrated that the light-triggered NO• release properties of **RuNO-5** can be nicely extended to two-photon activation.

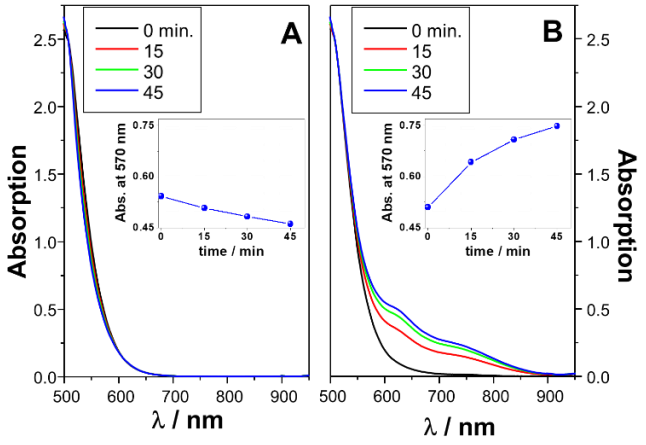

Figure 9. Evolution of the absorption spectrum of **RuNO-5** upon its two-photon irradiation at 980 nm. **A.** Without Griess agent (reference solution) **B.** With Griess agent. Insets: Time dependent changes of absorbance at 570 after each 15 min irradiation increment. Solvent : isovolume mixture of ACN / Water, [**RuNO-5**] = 0.3 mM, µ-volume cuvette with 2 mm optical path, P_{980nm} = 1.1 W.

Conclusion

The search of RuNO complexes able to release NO• under irradiation has been conducted in our group for about ten years. Initially restricted to monometallic species exhibiting σ_{TPA} values around 100 GM, the investigation of bimetallic species leads to a breakthrough with σ_{TPA} values higher than 1 500 GM in the best case (σ_{TPA}/MW~1.10 GM mol g^{-1}). These large TPA responses are in the order of magnitude of the most efficient TPA materials reported to date and are fully compatible with the therapeutic window of transparency, allowing applications as NO• donors in biological media. The present investigation proves the efficiency of terpyridine-based ligands to lead to bimetallic RuNO complexes with enhanced TPA efficiencies together with significant NO• release capabilities.

Experimental Section

Materials and equipment

All starting materials were obtained from Alfa-Aesar; the solvents were of analytical grade and used without further purification. Compounds **1a**,[42] **1b**,[43] **2a**,[20] **3**,[44] **5**,[45] **6**,[42] **9**,[46] **L1** (and related ruthenium complexes)[3] and **L3**,[4] were obtained following literature protocols; spectroscopic data were in good agreement. NMR spectra were recorded with a Bruker Avance III 300/400 spectrometers at 298 K using deuterated solvents; chemical shifts for ^{1}H- and ^{13}C-NMR data are relative to the residual nondeuterated solvent signal, fixed at δ = 7.26 ($CDCl_3$), δ = 1.940 (CD_3CN), δ = 3.310 ppm (MeOD) for ^{1}H-NMR and δ = 77.00 ($CDCl_3$), δ = 1.320 (CD_3CN) ppm for ^{13}C-NMR. ^{11}B-NMR spectra were recorded using $BF_3{\cdot}OEt_2$ as an external reference. Coupling constants (J) values are given in Hertz. Elemental analyses were performed at LCC using a PerkinElmer 2400 series II Instrument. Infrared spectra were recorded on a Perkin Elmer FTIR Frontier MIR/FIR spectrometer, using a diamond ATR. The UV-visible spectra were obtained on a Cary 60 UV-Visible spectrometer. HRMS data were acquired using an Xevo G2 Q TOF (Waters) UPLC spectrometer; for clarity "*M*" refers to the molecular ion in the case of organic molecules and neutral complexes or to the cation in the case of ionic coordination compounds.

The details for the synthesis of **[RuNO-2]**$(PF_6)_3$, **[RuNO-3]**$(PF_6)_6$, **[RuNO-4]**$(PF_6)_6$, and **[RuNO-5]**$(PF_6)_6$ are provided in supporting information.

Crystal structure determinations

Single crystals suitable for X-ray diffraction analysis were grown as follows: powdered [**RuNO-3**]$(PF_6)_6$ (3 mg) was dissolved in acetonitrile (2 mL). The filtered solution was placed in a large flask in the presence of a vial filled with a large amount of diethyl ether and set aside in the dark. The slow diffusion of diethyl ether into the acetonitrile solution led to the appearance of several crystals. The same procedure was employed for [**$RuNO_2$-3**]$(PF_6)_2$.

The data were collected on a Bruker Kappa Apex II diffractometer equipped with a 30 W air-cooled microfocus source using MoKα radiation (λ = 0.71073 Å) for [**RuNO-3**]$(PF_6)_6$ and on a Rigaku XtaLAB Synergy Dualflex diffractometer using a PhotonJet X-ray source (Cu, λ = 1.54184 Å) for [**$RuNO_2$-3**]$(PF_6)_2$. Oxford Cryosystems Cryostream cooling devices were used to collect the data at low

temperature (100(2) K). Phi and Omega scans were performed for data collection, an empirical absorption correction was applied and the structures were solved by intrinsic phasing method (ShelXT).[47] All non-hydrogen atoms were refined anisotropically by means of least-squares procedures on F^2 with ShelXL.[48] All the hydrogen atoms were refined isotropically at calculated positions using a riding model with their isotropic displacement parameters constrained to be equal to 1.5 times the equivalent isotropic displacement parameters of their pivot atoms for terminal sp^3 carbon and 1.2 times for all other carbon atoms. In both crystal structures, the SQUEEZE[49] function of PLATON was used to remove the electron density contribution of the highly disordered DMF molecules from the models. For [**RuNO-3**]$(PF_6)_6$, two PF_6^- anions are an occupancy of 0.5. Both crystal structures have been deposited with the Cambridge Crystallographic Data Center. Deposition Number(s) <url href="https://www.ccdc.cam.ac.uk/services/structures?id=doi:10.1002/chem.202201692"> CCDC 2168876 (for [**RuNO$_2$-3**]$(PF_6)_2$), and CCDC 2168877 (for [**RuNO-3**]$(PF_6)_6$)</url> contain(s) the supplementary crystallographic data for this paper. These data are provided free of charge by the joint Cambridge Crystallographic Data Centre and Fachinformationszentrum Karlsruhe <url href=" http://www.ccdc.cam.ac.uk/structures ">Access Structures service</url>.

Computational methods

The molecular structures were optimized using the Gaussian-09 program package[50] within the framework of the Density Functional Theory (DFT). The double-ζ basis set 6-31G* was used for all atoms except the heavy ruthenium atom, for which the LANL2DZ basis set was applied to account for relativistic effects.[51] To be consistent with our previous report on **[RuNO-1]$^{3+}$**,[20] we have selected the hybrid functional B3PW91 which has been shown to outperform other hybrid functionals (*e.g.* B3LYP) and pure functionals (*e.g.* PW91) in numerous cases of ruthenium complexes, especially when backbonding ligands (like NO) are present.[52,53] The vibrational analyses were performed at the same level to verify that the stationary points correspond to minima on the potential energy surfaces. The UV-visible electronic spectra were then computed at the CAM-B3LYP/6-31G* level, for consistency with our previous investigations.[20] This long-range corrected hybrid functional is also reported as being particularly well suited for studying molecules with very delocalized excited states.[54] Solvent effects were included in the optimization and computation of the UV-visible spectra by using the polarizable continuum model (PCM) implemented in Gaussian09 for acetonitrile (ε = 35.688). Molecular orbitals were plotted with GABEDIT 2.4.8.[55]

Before investigating **[RuNO-2]$^{3+}$** and **[RuNO-4]$^{6+}$**, in which two fluorene units are directly linked without any spacer, the most stable (either *cisoid* or *transoid*) conformation was investigated for a nonsubstituted bisfluorene molecule bearing 4 hexyl chains. The *cisoid* conformation was found to be the most stable one with difference in Gibbs free energy (ΔG) equal to 0.71 kcal mol^{-1}. Therefore, it was assumed that **[RuNO-2]$^{3+}$** and **[RuNO-4]$^{6+}$** exhibit the *cisoid* conformation. By contrast, the introduction of an alkyne C≡C linker between the fluorenes leads to the stabilization of the *transoid* geometry, which was therefore that assumed for **[RuNO-5]$^{6+}$**. Having this first result in hands, and to favor the convergence procedure, the hexyl chains were replaced by methyls in the five ruthenium complexes under investigation.

After first computations with symmetry constraints to test the C_2 and C_s geometries, **[RuNO-3]$^{6+}$** was found to adopt the more stable C_1 conformation, which is consistent with the X-ray structure. **[RuNO-4]$^{6+}$** was find C_2 within a tolerance of 0.0003 Å and **[RuNO-5]$^{6+}$** C_i within a tolerance of 0.0010 Å.

Consequently, the final computations were carried out assuming the strict geometry C_2 for **[RuNO-4]$^{6+}$**, and C_i for **[RuNO-5]$^{6+}$**.

Z-scan measurements

The Z-scan technique[20,56] was used to measure the nonlinear absorption coefficient of the samples in the wavelength range 700 – 1000 nm using short laser pulses of 80 fs at 1 kHz of repetition rate. The characterization at 800 nm was performed by the train of pulses delivered by a Ti:Sa amplifier (Libra HE from Coherent). For other wavelengths, the Z-scan method was implemented with an optical parametric amplifier (TOPAs, from Light Conversion). Molecules under study were dissolved in acetonitrile at different concentrations depending of the amount of sample available, in the range $1 – 5 \times 10^{-3}$ mol.L^{-1}. The nonlinear absorption of all samples was measured at different excitation energies. All samples were measured at least three times for each energy. To verify the measurements, the Z-scan apparatus was calibrated in closed aperture mode to measure the nonlinear refractive index n_2 of CS_2, obtaining values in the interval $1 – 2 \times 10^{-15}$cm^2/W, which is in very good agreement with the literature values; the dye rhodamine B (RB) (dissolved in methanol at a concentration of 1×10^{-2} M) was also measured in open aperture mode to compare the value of σ_{TPA} with the samples.[57] The TPA cross-section (σ_{TPA}) is obtained from the following expression equation:[58]

$$\sigma_{TPA} = \frac{\hbar\omega}{N}\beta \qquad (4)$$

Were N is the molecular density, ω the optical frequency, and β is the nonlinear absorption coefficient. The nonlinear coefficient β was calculated from the following equation:[56,59]

$$T(z) = 1 - \frac{1}{2\sqrt{2}}\beta\frac{I_0 L_{eff}}{1+(Z/Z_0)^2} \qquad (5)$$

where I_0 is the peak intensity, L_{eff} is the effective length of the sample with $L_{eff} = [1 - \exp(-\alpha_0 L)]/\alpha_0$, where L is the sample thickness and α_0 the absorption coefficient, Z the sample position and $Z_0 = (\pi\omega_0^2 / \lambda)$

Photochemistry

Photokinetic studies. Photokinetic studies on the photolysis reactions were carried out with a Cary 60 UV-Visible spectrophotometer equipped with a cooling water regulator. The temperature was maintained at 25 °C during the experiments. Irradiation was performed from a chassis wheeled wavelength-switchable LED source from Mightex Company. The sample solutions were placed in a quartz cuvette of 1 cm pathlength stirred continuously and the optical fiber was fixed laterally from it. The light intensity (5-6 mW) was measured with a power meter from Thorlabs. Absorption spectra were taken after each 10 seconds.

Quantum yield measurements: Light intensities (I_0) were determined before each photolysis experiments. The quantum yields (ϕ_{NO}) for the monometallic (**RuNO-1, RuNO-2**) and bimetallic (**RuNO-3**, **RuNO-4**, **RuNO-5**) complexes were determined by the program Sa3.3 written by D. Lavabre and V. Pimienta.[60] It allows the resolution of the differential equation (6):

$$\frac{d[A]}{dt} = -\Phi_{NO}\, I_a^A = -\Phi_{NO}\, Abs_A^\lambda I_0 F \qquad (6)$$

where I_a^A is the intensity of the light absorbed by the precursor; Abs_A^λ , the absorbance before irradiation; Abs_{Tot}^λ, the total absorbance; I_0, the incident intensity measured at 490 nm; and F, the photokinetic factor given by equation (7):

$$F = \frac{\left(1-10^{-Abs_{Tot}^\lambda}\right)}{Abs_{Tot}^\lambda} \qquad (7)$$

The equation was fitted with the experimental data $Abs_{Tot}^\lambda = f(t)$ and 2 parameters ϕ_{NO} and ε_B (ε_B is the molar extinction coefficient measured at the end of the reaction) at two wavelengths (λ_{irr} = 490 nm, λ_{obs}). λ_{obs} was chosen because it corresponds to a large difference between molar extinction coefficient at the initial and final time of the photochemical reaction. Simulation and optimization procedures were performed by using numerical integration and a non-linear minimization algorithm for the fitting of the model to the experimental data.[60,61] Detailed data are given in the supplementary material file.

EPR experiments

Electron paramagnetic resonance (EPR) spectra were collected on a Brucker ESP 500E (X band) spectrometer. N–methyl-D-glucamine dithiocarbamate previously synthesized[62] reacted with Mohr salts to get [$Fe(MGD)_2$]. 90 µl of 1mM of Ru(NO) complexes in acetonitrile were mixed with 10 µl of an aqueous solution of 20mM [$Fe(MGD)_2$] and injected into quartz capillaries. Samples were irradiated directly in the EPR cavity. The light source was a 250 W Oriel Hg lamp (Palaiseau, France). The light was passed through an Oriel WG 400 UV filter (Palaiseau, France, $\lambda > 400$ nm) and delivered via an optical fiber to the grid of the cavity.

Supporting Information: The Supporting Information (150 pages) include synthetic procedures, all experimental NMR, UV-vis and mass spectra, computed geometries, details of X-Ray data, NO˙ release experiments, Z-scan data, detailed description of the TD-DFT analyses for one and two-photon absorption.

Acknowledgments

The authors thank Consejo Nacional de Ciencia y Tecnologia (CONACyT) and Centre National de la Recherche Scientifique (CNRS) for financial support. This work has been performed within the framework of the LIA-LCMMC International Laboratory and the IRP-MCCM French-Mexican International Research Program. A.E.C. thanks CONACyT for the PhD scholarship (270200).

References

[1] L. J. Ignarro, G. M. Buga, K. S. Wood, R. E. Byrns, G. Chaudhuri, *Proc. Natl. Acad. Sci. USA* **1987**, *84*, 9265-9269.

[2] R. M. J. Palmer, A. G. Ferrige, S. Moncada, *Nature* **1987**, *327*, 524-526.

[3] (a) L. J. Ignarro, *Nitric Oxide Biology and Pathobiology*, Academic Press, San Diego, **2000**.
(b) B. Bonavida, *Nitric Oxide and Cancer: Prognosis, Prevention and Therapy*, Springer, New-York, **2010**.
(c) A. R. Butler, R. Nicholson, *Life Death and Nitric Oxide*, The Royal Society of Chemistry, Cambridge, **2003**.

[4] (a) P. C. Ford, *Nitric Oxide* **2013**, *34*, 56-64.
(b) A. W. Carpenter, M. H. Schoenfisch, *Chem. Soc. Rev.* **2012**, *41*, 3742-3752.

[5] S. Hossain, L. M. Nisbett, E. M. Boon, Discovery of two bacterial nitric oxide-responsive proteins and their roles in bacterial biofilm regulation. *Acc. Chem. Res.* **2017**, *50*, 1633– 163.

[6] J. C. Toledo Jr., O. Augusto, *Chem. Res. Toxicol.* **2012**, *25*, 975-989.

[7] I. Stepanenko, M. Zalibera, D. Schaniel, J. Telser, V. B. Arion, *Dalton Trans.* **2022**, 51, 5367-5393.

[8] (a) N. L. Fry, P. K. Mascharak, *Acc. Chem. Res.* **2011**, *44*, 289-298.
(b) M. J. Rose, P. K. Mascharak, *Coord. Chem. Rev.* **2008**, *252*, 2093-2114.

[9] R. Santana da Silva, R. Galvao de Lima, S. P. Machado, *Adv. Inorg. Chem.* **2015**, *67*, 265-294.

[10] for recent reports on ruthenium nitrosyl complexes with NO· releasing capabilities, see:
(a) A. Ferrarini, R. N. Soek, R. Rebecchi Rios, F. S. Santana, R. B. Campos, R. S. da Silva, F. S. Nunes, *Inorg. Chim. Acta* **2022**, *533*, 120771.
(b) J.-H. Cho, M. Kim, Y. You, H.-I. Lee, *Chem. Asian J.* **2022**, *17*, e202101244.
(c) I. Stepanenko, P. Mizetskyi, E. Orlowska, L. Bucinsky, M. Zalibera, B. Venosova, M. Clemancey, G. Blondin, P. Rapta, G. Novitchi, W. Schrader, D. Schaniel, Y.-S. Chen, M. Lutz, J. Telser, V. B. Arion, *Inorg. Chem.* **2022**, *61*, 950-967.
(d) N. Sharma, P. Arjunan, S. Marepally, N. Jain, A. R. Naziruddin, A. Ghosh, C. R. Mariappan, J. D. Amilan, *J. Photochem. Photobiol. A* **2022**, *425*, 113703.
(e) L. Song, H. Bai, Ch. Liu, W. Gong, A. Wang, L. Wang, Y. Zhao, X. Zhao, Xuan, H. Wang, *Molecules* **2021**, *26*, 2545.
(f) I. S. Fomenko, A. A. Mikhailov, V. Vorobyev, N. V. Kuratieva, G. A. Kostin, D. Schaniel, V. A. Nadolinny, A. L. Gushchin, *J. Photochem. Photobio. A* **2021** *407*, 113044.
(g) E. D. Stolyarova, A. A. Mikhailov, A. A. Ulantikov, J. A. Eremina, L. S. Klyushova, N. V. Kuratieva, V. A. Nadolinny, G. A. Kostin, *J. Photochem. Photobiol. A* **2021**, *421*, 113520.
(h) B. Giri, T. Saini, S. Kumbhakar, K, Selvan K., A. Muley, A. Misra, S. Maji, *Dalton Trans.* **2020**, *49*, 10772-10785.
(i) B. Giri, S. Kumbhakar, K. Selvan K, A. Muley, S. Maji, Somnath, *New J. Chem.* **2020**, *44*, 18732-18744.
(j) A. P. de Sousa, A. C. S. Gondim, E. H. S. de Souza, L. G. de Franca Lopes, E. H. Teixeira, M. A. Vasconcelos, P. H. R. Martins, E. J. T. Medeiros, A. A. Batista, A. K. M. Holanda, *New J. Chem.* **2020**, *44*, 21318-21325.
(k) Y. T. Yu, S. W. Shi, Y. Wang, Q. L. Zhang, S. H. Gao, S. P. Yang, J. G. Liu, *ACS Appl. Mater. Inter.* **2020**, *12*, 312-321.
(l) Y.-T. Yu, S.-W. Shi, Y. Wang, Q.-L. Zhang, S.-H. Gao, S.-P. Yang, J.-G. Liu, *ACS Appl. Mat. Interfaces* **2020**, *12*, 312-321.
(m) Q. Lin, G. Huile, *Asian J. Pharma. Sci.* **2019**, *14*, 380-390.
(n) Y.-H. Li, M. Guo, S.-W. Shi, Q.-L. Zhang, S.-P. Yang, J.-G. Liu, *J. Mater. Chem. B*, **2017**, *5*, 7831-7838.
(o) H.-J. Xiang, M. Guo, J.-G. Liu, *Eur. J. Inorg. Chem.* **2017**, 1586-1595.

[11] M. R. Hamblin, T. N. Demidova, *Proc. SPIE, Mechanism for Low-Light Therapy* **2006**, 6140, 614001–614012.

[12] For reviews on TPA molecular materials and applications, see:
(a) B. Strehmel, V. Strehmel, *Adv. Photochem.* **2007**, *29*, 111-341.
(b) G. S. He, L. S. Tan, Q. Zheng, P. N. Prasad, *Chem. Rev.* **2008**, *108*, 1245-1330.
(c) M. Pawlicki, H. A. Collins, R. G. Denning, H. L. Anderson, *Angew. Chem. Int. Ed.* **2009**, *48*, 3244-3266.

[13] For selected examples of TPA molecules with applications in photodynamic therapy, see:
(a) M. A. Oar, W. R. Dichtel, J. M. Serin, J. M. J. Fréchet, J. E. Rogers, J. E. Slagle, P. A. Fleitz, L. S. Tan, T. Y. Ohulchanskyy, M. N. Prasad, *Chem. Mater.* **2006**, *18*, 3682-3692.
(b) S. Kim, T. Y. Ohulchanskyy, H. E. Pudavar, R. K. Pandey, P. N. Prasad, *J. Am. Chem. Soc.* **2007**, *129*, 2669-2675.
(c) M. Khurana, H. A. Collins, A. Karotki, H. L. Anderson, D. T. Cramb, B. C. Wilson, *Photochem. Photobiol.* **2007**, *83*, 1441-1448.
(d) K. S. Samkoe, A. A. Clancy, A. Karotki, B. C. Wilson, D. T. Cramb, *J. Biol. Opt.* **2007**, 12, 034025/034021-034025/034014.
(e) J. R. Starkey, A. K. Rebane, M. A. Drobizev, F. Meng, A. Gong, A. Elliot, K. McInnerney, C. W. Spangler, *Clin. Cancer Res.* **2008**, *14*, 6564-6573.
(f) L. Beverina, M. Crippa, M. Landenna, R. Ruffo, P. Salice, F. Silvestri, S. Versari, A. Villa, L. Ciaffoni, E. Collini, C. Ferrante, S. Bradamante, C. M. Mari, R. Bozio, G. A. Pagani, *J. Am. Chem. Soc.* **2008**, *130*, 1894-1902.
(g) H. A. Collins, M. Khurana, E. H. Moriyama, A. Mariampillai, E. Dahlstedt, M. Balaz, M. K. Kuimova, M. Drobizhev, V. X. D. Yang, D. Phillips, A. Rebane, B. C. Wilson, H. L. Anderson, *Nat. Photonics* **2008**, *2*, 420-424.

[14] For recent reports on TPA materials containing fluorene units, see : (a) S. Abid, Ch. Nguyen, M. Daurat, D. Durand, B. Jamoussi, M. Blanchard-Desce, M. Gary-Bobo, O. Mongin, Ch. O. Paul-Roth, F. Paul, *Dyes and Pigments* **2022**, *197*, 109840. (b) C. Benitez-Martin, S. Li, A. Dominguez-Alfaro, F. Najera, E. Perez-Inestrosa, U. Pischel, J. Andreasson, *J. Am. Chem. Soc.* **2020**, *142*, 14854-14858. (c) S. Goswami, S. Cekli, E. Alarousu, R. W. Winkel, M. Younus, O. F. Mohammed, K. S. Schanze, Macromolecules **2020**, *53*, 6279-6287. (d) J.-W. Choi, S.-H. Choi, S. T. Hong, M. S. Kim, S. S. Ryu, Y. U. Yoon, K. C. Paik, M. S. Han, T. Sim, B. R. Cho, *Chem. Commun.* **2020**, *56*, 3657-3660. (e) K. K. Guzman-Rabadan, M. Guizado-Rodriguez, V. Barba, M. Rodriguez, J. Velusamy, G. Ramos-Ortiz, *Opt. Mater.* **2020**, *101*, 109758. (f) W. Wang, Y. Liu, J. Niu, W. Lin, *J. Fluoresc.* **2019**, *29*, 1457-1465. (g) S. Oger, D. Schapman, R. Mougeot, S. Leleu, N. Lascoux, P. Baldeck, M. Benard, Th. Gallavardin, L. Galas, X. Franck, *Chem. Eur. J.* **2019**, *25*, 10954-10964. (h) A. Sourdon, M. Gary-Bobo, M. Maynadier, M. Garcia, J.-P. Majoral, A.-M. Caminade, O. Mongin, M. Blanchard-Desce, Mireille, *Chem. Eur. J.* **2019**, *25*, 3637-3649. (i) B. Zhai, W. Hu, R. Hao, W. Ni, Z Liu, *Analyst* **2019**, *144*, 5965-5970.

[15] A. Enriquez-Cabrera, P.G. Lacroix, I. Sasaki, S. Malet-Ladeira, N. Farfan, R.M. Barba-Barba, G. Ramos-Ortiz, I. Malfant, *Eur. J. Inorg. Chem.* 2018, 531-543.

[16] V. Bukhanko, A. F. León-Rojas, P. G. Lacroix, M. Tassé, G. Ramos-Ortiz, R. M. Barba-Barba, N. Farfán, R. Santillan, I. Malfant, *Eur. J. Inorg. Chem.* 2021, 1670-1684.

[17] M. Romero Ávila, A. F. León-Rojas, P. G. Lacroix, I. Malfant, N. Farfán, R. Mhanna, R. Santillan, G. Ramos-Ortiz, J.-P. Malval, *J. Phys. Chem. Lett.* **2020**, *11*, 6487-6491

[18] F. Kröhnke, W. Zecher, J. Curtze, D. Drechsler, K. Pfleghar, K. E. Schnalke, W. Weis, *Angew. Chem. Int. Ed. Eng.* **1962**, *1*, 626-632.

[19] (a) A. Jouaiti, *Synth. Commun.* **2021**, *51*, 1547-1555. (b) P. Labra-Vázquez, M. Bocé, M. Tassé, S. Mallet-Ladeira, P. G. Lacroix, N. Farfán, I. Malfant, *Dalton Trans.* **2020**, *49*, 3138-3154. (c) J. Wang, G. S. Hanan, *Synlett* **2005**, *2005*, 1251-1254.

[20] A. Enriquez-Cabrera, I. Sasaki, V. Bukhanko, M. Tassé, S. Mallet-Ladeira, P. G. Lacroix, R. M. Barba-Barba, G. Ramos-Ortiz, N. Farfán, Z. Voitenko, I. Malfant, *Eur. J. Inorg. Chem.* **2017**, *2017*, 1446-1456.

[21] Z. Ji, S. Li, Y. Li, W. Sun, *Inorg. Chem.* **2010**, *49*, 1337-1346.

[22] M. Zalas, B. Gierczyk, M. Cegłowski, G. Schroeder, *Chem. Papers* **2012**, *66*, 733-740.

[23] M. Pittelkow, J. B. Christensen, *Org. Lett.* **2005**, *7*, 1295-1298.

[24] X. Chen, L. Ma, Y. Cheng, Z. Xie, L. Wang, *Polymer Internat.* **2007**, *56*, 648-654.

[25] G. K Lahiri, W. Kaim, *Dalton Trans.*, **2010**, *39*, 4471-4478.

[26] A. D. Laurent, D. Jacquemin, *Int. J. Quant. Chem.* **2013**, *113*, 2019-2039.

[27] E.W. Van Stryland, M. Sheik-Bahae, in *Characterization Techniques and Tabulations for Organic Nonlinear Material*s (Eds.: M.G. Kuzyk, C.W. Dirk), marcel Dekker, Inc., 1998, p.655-682.

[28] (a) L. Wu, J. Liu, P. Li, B. Tang Bo, T.D. James Tony, *Chem. Soc. Rev.*, **2021**, *50*, 702-734. (b) C. Xu, W. W. Webb, *J. Opt. Soc. Am. B*, **1996**, *13*, 481–491.

[29] M. Roose, I. Sasaki, V. Bukhanko, S. Mallet-Ladeira, R. M. Barba-Barba, G. Ramos-Ortiz, A. Enriquez-Cabrera, N. Farfán, P. G. Lacroix, I. Malfant**,** *Polyhedron*, **2018**, 151, 100-111.

[30] (a) J. M. Hales, D. J. Hagan, E. W. Van Stryland, K. J. Schafer, A. R. Morales, and K. D. Belfield, P. Pacher, O. Kwon, E. Zojer, J. L. Bredas, *J. Chem. Phys*. **2004**, 121, 3152-3160. (b) M. Drobizhev, A. Karotki, M. Kruk, A. Rebane, *Chem. Phys. Lett*. **2002**, 355, 175–182.

[31] M. Albota, D. Beljonne, J. L. Brédas, J. E. Ehrich, J. Y. Fu, A. A. Heikal, S. E. Hess, T. Kogej, M. D. Levin, S. R. Marder, D. MacCord-Maughon, J. W. Perry, H. Röckel, M. Rumi, G. Subbramaniam, W. W. Webb, X. L. Wu, C. Xu, *Science* **1998**, *281*, 1653-1656.

[32] B. J. Orr, J. F. Ward, *Mol. Phys.*, **1971**, *20*, 513-526.

[33] F. Terenziani, C. Katan, E. Badaeva, S. Tretiak, M. Blanchard-Desce, *Adv. Mater.*, **2008**, *20*, 4641-4678.

[34] (a) P. N. Prasad, D. J. Williams Eds. *Nonlinear Optical Effects in Molecules and Polymers*, Wiley, New York 1991. (b) D.S. Chemla, J. Zyss Eds. *Nonlinear Optical Properties of Organic Molecules and Crystals*, Academic Press, New York, 1987.

[35] (a) B. Strehmel, A. M. Sarker, H. Detert, *ChemPhysChem*, **2003**, *4*, 249-259. (b) M. Rumi, J. E. Ehrlich, A. A. Heikal, J. W. Perry, S. Barlow, Z. Y. Hu, D. McCord-Maughon, T. C. Parker, H. Rockel, S. Thayumanavan, S. R. Marder, D. Beljonne, J. L. Bredas, J. Am. Chem. Soc. 2000, 122, 9500-9510.

[36] P. V. Simpson, L. A. Watson, A. Barlow, G. Wang, M. P. Cifuentes, M. G. Humphrey, *Angew. Chem. Int. Ed.* **2016**, *55*, 2387-2391.

[37] (a) I. Sasaki, S. Amabilino, S. Mallet-Ladeira, M. Tassé, A. Sournia-Saquet, P. G. Lacroix, I. Malfant, *New J. Chem.* **2019**, *43*, 11241-11250.
(b) M. Roose, M. Tassé, Marine, P. G. Lacroix, I. Malfant, *New J. Chem.* **2019**, *43*, 755-767.
(c) V. Bukhanko, P. G. Lacroix, I. Sasaki, M. Tassé, Z. Voitenko, I. Malfant, *Inorg. Chim. Acta* **2018**, 482, 195-205.
(d) J. Akl, I. Sasaki, P. G. Lacroix, I. Malfant, S. Malet-Ladeira, P. Vicendo, N. Farfan, R. Santillan, Dalton Trans., 2014, 43, 12721-12733.

[38] S. Amabilino, M. Tasse, P. G. Lacroix, S. Mallet-Ladeira, V. Pimienta, J. Akl, I. Sasaki, I. Malfant, *New, J. Chem.* **2017**, *41*, 7371-7383.

[39] A. J. Liu, Q. Duan, J. Wang, Z. Song, X. Qiao, H. Wang, *J. Biomed. Opt.*, **2015**, *20*, 015004-1 - 015004-7.
[40] D. Tsikas, *J. Chromatogr. B* **2007**, *851*, 51-70.
[41] J. Akl, I. Sasaki, P. G. Lacroix, V. Hugues, M. Bocé, S. Mallet-Ladeira, P. Vicendo, M. Blanchard-Desce, I., Malfant, *Photochemical & Photobiological Sciences*, **2016**, *15*, 1484-1491
[42] S. Barik, W. G. Skene, *European Journal of Organic Chemistry* **2013**, *2013*, 2563-2572.
[43] J. Massin, L. Ducasse, M. Abbas, L. Hirsch, T. Toupance, C. Olivier, *Dyes and Pigments* **2015**, *118*, 76-87.
[44] P. Labra-Vázquez, M. Palma-Contreras, R. Santillan, N. Farfán, *Journal of Molecular Structure* **2017**, *1131*, 156-162.
[45] A. P. Kulkarni, X. Kong, S. A. Jenekhe, *The Journal of Physical Chemistry B* **2004**, *108*, 8689-8701.
[46] Y. Tian, W.-C. Wu, C.-Y. Chen, T. Strovas, Y. Li, Y. Jin, F. Su, D. R. Meldrum, A. K. Y. Jen, *Journal of Materials Chemistry* **2010**, *20*, 1728-1736.
[47] ShelXT, G. M. Sheldrick, University of Göttingen, *Acta Crystallogr. Sect. A*, **2015**, *71*, 3-8.
[48] ShelXL, G. M. Sheldrick, University of Göttingen, *Acta Crystallogr. Sect. C*, **2015**, *71*, 3-8.
[49] A. L. Spek, *Acta Crystallogr. Sect. C*, **2015**, 71, 9-18.
[50] Gaussian 09, Revision E.01, M. J. Frisch, G. W. Trucks, H. B. Schlegel, G. E. Scuseria, M. A. Robb, J. R. Cheeseman, G. Scalmani, V. Barone, B. Mennucci, G. A. Petersson, H. Nakatsuji, M. Caricato, X. Li, H. P. Hratchian, A. F. Izmaylov, J. Bloino, G. Zheng, J. L. Sonnenberg, M. Hada, M. Ehara, K. Toyota, R. Fukuda, J. Hasegawa, M. Ishida, T. Nakajima, Y. Honda, O. Kitao, H. Nakai, T. Vreven, J. A. Montgomery, Jr., J. E. Peralta, F. Ogliaro, M. Bearpark, J. J. Heyd, E. Brothers, K. N. Kudin, V. N. Staroverov, R. Kobayashi, J. Normand, K. Raghavachari, A. Rendell, J. C. Burant, S. S. Iyengar, J. Tomasi, M. Cossi, N. Rega, J. M. Millam, M. Klene, J. E. Knox, J. B. Cross, V. Bakken, C. Adamo, J. Jaramillo, R. Gomperts, R. E. Stratmann, O. Yazyev, A. J. Austin, R. Cammi, C. Pomelli, J. W. Ochterski, R. L. Martin, K. Morokuma, V. G. Zakrzewski, G. A. Voth, P. Salvador, J. J. Dannenberg, S. Dapprich, A. D. Daniels, Ö. Farkas, J. B. Foresman, J. V. Ortiz, J. Cioslowski, D. J. Fox, Gaussian, Inc., Wallingford CT, 2009.
[51] (a) P. J. Hay, W. R. Wadt, *J. Chem. Phys.* **1985**, *82*, 270-283. (b) W. R. Wadt, P. J. Hay, *J. Chem. Phys.* **1985**, *82*, 284-298. (c) P. J. Hay, W.R. Wadt, *J. Chem. Phys.* **1985**, *82*, 299-310.
[52] M. J. Rose, P. K. Mascharak, *Inorg. Chem.* **2009**, *48*, 6904-6917.
[53] P. Hirva, M. Haukka, M. Jaconen, *J. Mol. Model.* **2008**, *14*, 171-181.
[54] D. Jacquemin, E. A. Perpète, G. E. Scuseria, I. Ciofini, C. Adamo, *J. Chem. Theory Comput.* **2008**, *4*, 123-135
[55] http://sites.Google.com/site/allouchear/Home/gabedit.
[56] E.W. Van Stryland, M. Sheik-Bahae, in *Characterization Techniques and Tabulations for Organic Nonlinear Material*s (Eds.: M.G. Kuzyk, C.W. Dirk), Marcel Dekker, Inc., 1998, p.655-682.
[57] N. S. Makarov, M. Drobizhev, A. Rebane, Opt. Express **2008**, *16*, 4029-4047.
[58] M. Albota, D. Beljonne, J. L. Brédas, J. E. Ehrich, J. Y. Fu, A. A. Heikal, S. E. Hess, T. Kogej, M. D. Levin, S. R. Marder, D. MacCord-Maughon, J. W. Perry, H. Röckel, M. Rumi, G. Subbramaniam, W. W. Webb, X. L. Wu, C. Xu, *Science* **1998**, *281*, 1653–1656.
[59] M. Sheik-Bahae, A. A. Said, T. H. Wei, D. J. Hagan, E. W. Van Stryland, *IEEE J. Quant. Electron.* **1990**, *26*, 760-769.
[60] Program Sa3.3 written by D. Lavabre and V. Pimienta (http://cinet.chim.pagesperso-orange.fr/tele_sa/install_Sa.html).

[61] V. Pimienta, C. Frouté, M.-H. Deniel, D. Lavabre, R. Guglielmetti, J. -C. Micheau, *J. Photochem. Photobiol. A,* **1999**, *122* 199-204 (reference 35).
[62] L. A. Shinobu, S. G. Jones, M. M. Jones *Acta Pharmacol. Et Toxicol*. 1984, **54**, 189-194.

Table of contents

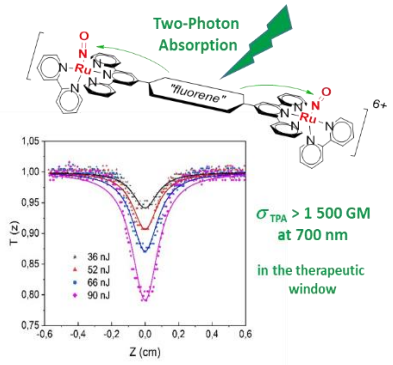

Text: A series of bimetallic RuNO complexes with quadrupolar electronic structures exhibit TPA cross-section up to 1523 GM under irradiation at λ = 700 nm, in the therapeutic window of transparency of biological tissues. The biologically active nitric oxide radical (NO$^{\bullet}$) is released in any case.